This article has been accepted for publication in a future issue of this journal, but has not been fully edited. Content may change prior to final publication. Citation information: DOI 10.1109/TCOMM.2015.2438813, IEEE Transactions on Communications

Symbol Error Rate of MPSK over EGK Channels Perturbed by a Dominant Additive Laplacian Noise

Hamza Soury, *Student Member, IEEE*, and Mohamed-Slim Alouini, *Fellow, IEEE*

***Abstract*—The Laplacian noise has received much attention during the recent years since it affects many communication systems. We consider in this paper the probability of error of an M-ary phase shift keying (PSK) constellation operating over a generalized fading channel in presence of a dominant additive Laplacian noise. In this context, the decision regions of the receiver are determined using the maximum likelihood and the minimum distance detectors. Once the decision regions are extracted, the resulting symbol error rate expressions are computed and averaged over an Extended Generalized-K fading distribution. Generic closed form expressions of the conditional and the average probability of error are obtained in terms of the Fox's H function. Simplifications for some special cases of fading are presented and the resulting formulas end up being often expressed in terms of well known elementary functions. Finally, the mathematical formalism is validated using some selected analytical-based numerical results as well as Monte-Carlo simulation-based results.**

***Index Terms*—Symbol error rate, phase shift keying modulation, Laplacian noise, maximum likelihood, minimum distance, extended generalized-K fading, Nakagami-*m* fading, Rayleigh, fading.**

I. Introduction

The Laplacian noise (LN) has pinched research interest for a long time for its properties. It is widely used and is indeed quite popular in signal processing, signal detection, and communication studies to model impulsive noise [1]–[3]. As mentioned in [4], the impulsive ambient noise, and behind it the Laplacian noise, can model among others thunder and lightning, ice avalanches, all kinds of machine motors, neon signs, etc. Moreover, in [5] it was proven that the noise in long range communication is no longer Gaussian and has an impulsive nature. Figure [5, Fig.10] shows that the PDF of the noise in the discrete time model is similar to the Laplacian distribution. It is claimed also that the non-Gaussian behavior of the noise has important implications on the receiver design and on the evaluation of the system performance. In other words, if the system is designed on the mistaken assumption that the noise is Gaussian while it is actually not, then the probability of error could be much greater than expected.

Actually, many communication systems in which the LN is applicable, can be found in the literature. For example in the ultra-wide bandwidth (UWB) wireless systems, the multi-user interference can be modeled by the Laplacian distribution [6]–[13]. Furthermore, the LN was studied by Kamboj *et al.* [14] in a free-space optics (FSO) communication context as a non Gaussian noise. In another area of research, Beaulieu *et al.* built an optimal detector for LN [15], [16], and studied some properties of the LN by computing the bit error rate of binary data [17]. Finally, works in [18] and [19] dealt with detection problems in LN environment. More specifically, most of those previous works are dealing with the bit error rate of binary phase shift keying (BPSK) constellation for different system models. Beaulieu and Young are studying some optimal detectors in LN using different filter structure for UWB systems. In fact, their aim is to search the best optimal filter (either matched filter or other filter) to get lower bit error rate for a BPSK constellation in this environment. On the other hand, Kamboj *et al.* focused on getting the probability of false alarm in FSO systems in presence of slow Rayleigh fading. Thereby, our contribution consists on computing the symbol error rate (SER) of M-ary phase shift keying (MPSK) constellation in presence of additive LN. Also we aim to get a closed form of the average SER over a generalized fading channel such that the EGK fading distribution for which many fading distributions such as Rayleigh and Nakagami-m are special cases of it.

It should be noted at this point that the SER of MPSK has been extensively studied in the case of the additive Gaussian noise (GN) [20] and as a result different expressions including integral forms and approximations were derived. It should be noted that in the case of the GN environment, the maximum likelihood (ML) detector coincides with the minimum distance (MD) detector due to the quadratic form of the Gaussian distribution.

In this paper, we consider a channel with additive white Laplacian noise (AWLN). In this case, the ML detector differs from the MD detector, as shown initially by the authors in the conference version of this paper [21]. We present, in this paper, the decision regions corresponding to the ML detector and derive the SER of M-PSK using both the ML and MD detectors. Also note that we are modeling the noise at the output of the filter without going through the processing before the detector as done in [14], [22]. According to the work done in [21], the present article acts as an extension of that work. In fact the present work deals with (i) decision regions of MPSK using an L_1 norm detector in presence of Laplacian noise, (ii) the conditional/average SER derived using the L_1 norm detector, and (iii) a study of the asymptotic results at high SNR, which were not presented in the conference version of this work [21]. Besides the additive noise, it is assumed that the communication is affected also by a fluctuation that behaves as a flat fading, which is modeled by an extended generalized-$\mathcal{K}$ (EGK) composite fading distribution [23]. The EGK distribution is a versatile distribution that covers a wide variety of well known fading distributions as special cases or limit cases [24]. Hence the previously obtained conditional

H. Soury and M.-S. Alouini are with King Abdullah University of Science and Technology (KAUST), Thuwal, Makkah Province, Kingdom of Saudi Arabia. The authors are members of the KAUST Strategic Research Initiative (SRI) in Uncertainty Quantification. E-mail: {soury.hamza, slim.alouini}@kaust.edu.sa.

This article has been accepted for publication in a future issue of this journal, but has not been fully edited. Content may change prior to final publication. Citation information: DOI 10.1109/TCOMM.2015.2438813, IEEE Transactions on Communications

SER is averaged over the multiplicative fading distribution in order to get the desired average SER (ASER).

The contributions of this paper are

- Presentation of the decision regions of MPSK perturbed by Laplacian noise using an L_1 norm detector
- Computation of the conditional SER of MPSK subject to Laplacian noise
- Derivation of closed-form expressions for the average SER over an EGK channel and simplified expressions for some special cases
- Development of the asymptotic results of the average SER at high SNR.

The remaining content of this paper is organized as follows. In section II, the detection regions of MPSK constellation are described and presented for both detectors (ML and MD). Next, the conditional SER is evaluated in section III and generic expressions for both detectors are derived. Subsequently, the SER is averaged over the EGK fading distribution in section IV and some special cases of the fading distribution covered by the EGK are presented also in this section. Finally, section V presents some numerical results and their discussion before including some concluding remarks in section VI.

II. Detection Regions in Laplacian noise

A. Discrete Time Model

Studies of multiple access interference (MAI) in time hopping (TH) UWB were conducted in [1]–[3], [6]–[10], [13]. In [7], an accurate evaluation of the multiple access performance in TH-PPM and TH-UWB systems was conducted. Actually, the PDF of the sum of the interference and the Gaussian noise in the discrete time model was established. The results of [3] show that this PDF can not be a Gaussian distribution (see [7, Fig.2 and Fig.3]). An approximation of that PDF was made in [1], [6], where Beaulieu *et al.* proved that the cumulative MAI in the discrete time model can be modeled as a Laplacian distribution for TH-UWB systems. In fact in [1, Fig.2], the authors have shown that the PDF of the multiple interference, coming form the multi-user, can be approximated by the Laplacian PDF. More specifically, the tail of the simulated PDF (real one) is near the Laplacian PDF tail. Moreover, in [6], the authors proved that the MAI in discrete time model can be modeled as an additive noise which can not be a Gaussian distribution. Actually they experiment three types of distributions, one of them is the Laplacian distribution which shows a better fit than the Gaussian approximation for the MAI as shown in [6, Fig.1].

Moreover, Dhibi *et al.* studied the impulsiveness of the multi user interference (MUI) in UWB systems in [2], [3]. In [2] they presented a mathematical proof of the impulsiveness of the MUI after filtering [2, Eq. 18]. Actually they mentioned that PDF of the MUI describes the so-called Middleton Class A (MCA) noise, which is an impulsive noise distribution. In our model, one may replace the MCA distribution by the Laplacian distribution.

To conclude, all of these works [1]–[3], [6]–[8] have studied the discrete time model of an UWB system with MUI. They proved that the MAI (or the MUI), in discrete time model, can be modeled as a Laplacian noise and that the thermal noise component can be neglected. These previous studies were made for UWB systems. Nevertheless, our model is applicable for any system using the same discrete time model we are using and is as such not limited to UWB systems.

On the other hand, the linear filter is no longer optimal in presence of laplacian noise as proved in [25], where in [25, Fig.5 and Fig.6] the optimal filter has better performance than the linear filter. Actually, the superiority of the soft limiting receiver, built in [1], over the matched filter is intuitive, as mentioned in [1].

B. System Model

Let us consider a single input single output (SISO) communication system. $\mathcal{S}$, the transmitted signal, is mapped according to an MPSK constellation, where M is a power of 2. The symbols are distributed uniformly over the circle with radius $\sqrt{E_S}$, defined as the energy per symbol, all symbols are equiprobable. The mathematical model of the system is given by

$$\mathcal{R} = \mathcal{H}\,\mathcal{S} + \mathcal{N}, \tag{1}$$

where $\mathcal{S}$ is multiplied by a channel fading coefficient (envelope) $\mathcal{H} \in \mathbb{R}^+$ and added to a Laplacian noise $\mathcal{N}$. In (1), $\mathcal{R}$ denotes the received signal. $\mathcal{S}$, $\mathcal{N}$, and $\mathcal{R}$ have two components (in-phase and quadrature phase components), in other words $\mathcal{S}$, $\mathcal{N}$, and $\mathcal{R}$ are complex scalars. In this work, we assume that the channel fading envelope has generalized flat fading characteristics. Furthermore, the noise is considered as Laplacian noise with zero mean and one side power spectral density $\sigma^2 = N_0/2$. More specifically, the probability density function (PDF) of a Laplacian random variable is defined as [17]–[19]

$$X \sim \mathcal{L}(\mu,\sigma) \quad , \quad f_X(x;\mu,\sigma) = \frac{1}{\sqrt{2}\sigma} e^{-\sqrt{2}\frac{|x-\mu|}{\sigma}}, \tag{2}$$

where μ represents the location parameter and is equal to the mean, while σ is the variance.

In the following analysis of the detection regions, the system performance is conditioned over the instantaneous received signal to noise ratio (SNR) γ, which is defined as

$$\gamma = \frac{\mathcal{H}^2 E_{\mathcal{S}}}{N_0}. \tag{3}$$

Without loss of generality, we normalize $\mathcal{S}$ in (1) by dividing it by $\mathcal{H}\sqrt{E_S}$. The resulting normalized system model is given by

$$r = s + n, \tag{4}$$

where s has a unit energy per symbol and n has a variance equal to $\frac{1}{\gamma}$.

The in-phase component is indexed by I, while the quadrature phase component is indexed by Q in all signals. Indeed, (s_I, s_Q) are the components of s, (n_I, n_Q) are the components of n, and (I, Q) are the received components. The components of the normalized system model can be re-written as

$$\begin{cases} I &= s_I + n_I \\ Q &= s_Q + n_Q. \end{cases} \tag{5}$$

This article has been accepted for publication in a future issue of this journal, but has not been fully edited. Content may change prior to final publication. Citation information: DOI 10.1109/TCOMM.2015.2438813, IEEE Transactions on Communications

Note that n_I and n_Q are independent random variables that follow a Laplacian distribution with zero mean and variance $\frac{1}{2\gamma}$ each. Therefore, (I, Q) can be modeled as two independent Laplacian random variables with mean (s_I, s_Q) and variance $\frac{1}{2\gamma}$ each. From (2), the joint PDF of (I, Q) can thus be written as

$$f_{IQ}(I,Q) = \gamma e^{-2\sqrt{\gamma}(|I-s_I|+|Q-s_Q|)}, \quad \forall I, Q \in \mathbb{R}. \tag{6}$$

C. Maximum Likelihood Detector

The transmitted symbols are distributed uniformly over the unit circle, which means that $(s_I^k, s_Q^k) = (\cos(\phi), \sin(\phi))$, where $\phi = \frac{2k\pi}{M}$ and $k \in 0, 1 \dots M-1$.

Consider two equiprobable symbols $s^\phi = (s_I^\phi, s_Q^\phi)$ and $s^\theta = (s_I^\theta, s_Q^\theta)$ with angles ϕ and θ. In what follows, we will refer to the angles instead of the signal to mention the desired symbol. Since the angles are equally likely, the maximum a posteriori (MAP) probability detector coincides with the ML detector. Thereby, the detector decides ϕ if $f_{IQ}(I, Q|\phi, \gamma) > f_{IQ}(I, Q|\theta, \gamma)$. In other words the following condition should be satisfied to decide ϕ instead of θ

$$|I - \cos(\phi)| + |Q - \sin(\phi)| < |I - \cos(\theta)| + |Q - \sin(\theta)|. \tag{7}$$

This condition can be also re-written using the L_1 norm as $\| r - s^\phi \|_1 < \| r - s^\theta \|_1$. It is obvious that this condition is similar to the known minimum euclidian distance condition (in particular in the Gaussian noise case). However instead of using the euclidian distance, the rule deploys the L_1 norm distance to detect the better angle (symbol). In this part, we focus on the detection using the L_1 norm, which corresponds to the ML detector.

1) 8-PSK: Consider for example an 8-PSK constellation shown in Fig. 1. In this example, we will produce the decision regions of the 8-PSK and draw it. Considering the symmetric properties of the PDF of the received signal $f_{IQ}(I, Q)$, we can focus only on the quarter of the plane lying between the I axis and the Q axis, where $\phi \in [0, \frac{\pi}{2}]$. Afterwards, we are focusing on the decision boundaries between s_0, s_1, and s_2.

From (7), we decide $\phi = 0$ (instead of $\phi = \frac{\pi}{4}$) when

$$|I - 1| + |Q| < \left| I - \frac{\sqrt{2}}{2} \right| + \left| Q - \frac{\sqrt{2}}{2} \right|. \tag{8}$$

To solve this inequality, three intervals appear according to the value of I, which are $I < \frac{\sqrt{2}}{2}$, $\frac{\sqrt{2}}{2} \leq I < 1$, and $1 \leq I$. The same analysis appears when dealing with the decision boundaries between $\phi = \frac{\pi}{4}$ and $\phi = \frac{\pi}{2}$, but the intervals appear according to the value of Q. Note that the region near the origin $(0, 0)$ is a conflict zone between $\phi = 0$ and $\phi = \frac{\pi}{2}$ which need to be studied separately. Near the origin, (7) can be simplified, and we decide $\phi = 0$ when $Q < I$.

Finally, the decision boundaries between $\phi = 0$, $\phi = \frac{\pi}{4}$, and $\phi = \frac{\pi}{2}$, can be written as

$$\begin{cases} \text{If} \quad I \in [0, \frac{\sqrt{2}-1}{2}] & \begin{cases} \phi = 0 \text{ if} & Q < I \\ \phi = \frac{\pi}{2} \text{ if} & Q \geq I \end{cases} \\ \text{if} \quad I \in [\frac{\sqrt{2}-1}{2}, \frac{1}{2}] & \begin{cases} \phi = 0 \text{ if} & Q < \frac{\sqrt{2}-1}{2} \\ \phi = \frac{\pi}{4} \text{ if} & \frac{\sqrt{2}-1}{2} \leq Q < I + \frac{1}{2} \\ \phi = \frac{\pi}{2} \text{ if} & I + \frac{1}{2} \leq Q \end{cases} \\ \text{if} \quad I \in [\frac{1}{2}, \frac{\sqrt{2}}{2}] & \begin{cases} \phi = 0 \text{ if} & Q < \frac{\sqrt{2}-1}{2} \\ \phi = \frac{\pi}{4} \text{ if} & \frac{\sqrt{2}-1}{2} \leq Q \end{cases} \\ \text{if} \quad I \in [\frac{\sqrt{2}}{2}, 1] & \begin{cases} \phi = 0 \text{ if} & Q < I - \frac{1}{2} \\ \phi = \frac{\pi}{4} \text{ if} & I - \frac{1}{2} \leq Q \end{cases} \\ \text{if} \quad I \in [1, +\infty[& \begin{cases} \phi = 0 \text{ if} & Q < \frac{1}{2} \\ \phi = \frac{\pi}{4} \text{ if} & \frac{1}{2} \leq Q. \end{cases} \end{cases} \tag{9}$$

The symmetric of these decision boundaries relative to the I axis and Q axis, construct the decision regions of the remaining 3 quarters of the plan to get the decision boundaries for all symbols. These boundaries are drawn in Fig. 1.

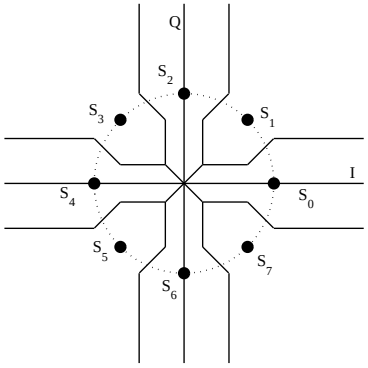

Fig. 1: Signal constellation and decision regions using the ML rule for 8-PSK.

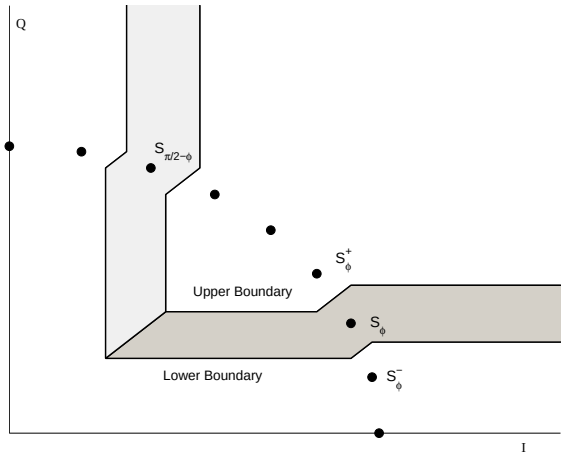

Fig. 2: Decision regions of two complementary angles ϕ and $\frac{\pi}{2} - \phi$.

This article has been accepted for publication in a future issue of this journal, but has not been fully edited. Content may change prior to final publication. Citation information: DOI 10.1109/TCOMM.2015.2438813, IEEE Transactions on Communications

2) General MPSK: The analysis of the decision boundaries in the general case of MPSK is more complicated. To simplify the procedure, we can find first the decision region of an angle ϕ and its complementary angle $\frac{\pi}{2}-\phi$ together (for example (S_0 and S_4) and (S_1 and S_3) in Fig. 3). Then the boundary between these two angle is the first bisector (line with equation $Q=I$). More specifically, it is easier to begin by finding the decision boundary between two adjacent angles ϕ and θ lying between 0 and $\frac{\pi}{4}$ with $\phi>\theta$. Hence to decide ϕ, condition (7) should be satisfied. In more details the decision between ϕ and θ can be summarized as follows

$$\begin{cases} \text{If} \quad I\in[\frac{c_\phi+s_\phi+s_\theta-c_\theta}{2},c_\phi] & \begin{cases}\theta \text{ if} \quad Q<\frac{c_\phi+s_\phi+s_\theta-c_\theta}{2}\\ \phi \text{ if} \quad Q\geq\frac{c_\phi+s_\phi+s_\theta-c_\theta}{2}\end{cases}\\ \text{if} \quad I\in[c_\phi,c_\theta] & \begin{cases}\theta \text{ if} \quad Q<I+\frac{s_\theta+s_\phi-c_\theta-c_\phi}{2}\\ \phi \text{ if} \quad Q\geq I+\frac{s_\theta+s_\phi-c_\theta-c_\phi}{2}\end{cases}\\ \text{if} \quad I\in[c_\theta,+\infty[& \begin{cases}\theta \text{ if} \quad Q<\frac{s_\theta+c_\theta+s_\phi-c_\phi}{2}\\ \phi \text{ if} \quad Q\geq\frac{s_\theta+c_\theta+s_\phi-c_\phi}{2}\end{cases}\end{cases} \tag{10}$$

where $c_x=\cos(x)$ and $s_x=\sin(x)$ for any angle x.

Given the previous analysis, the decision boundaries of ϕ and $\frac{\pi}{2}-\phi$ are described in Fig. 2. In fact, in Fig. 2 the lower boundary (between S_ϕ^- with angle ϕ^- and S_ϕ^+ with angle ϕ^+) is obtained with substituting θ by ϕ^- in (10), where the upper boundary is obtained with replacing ϕ by ϕ^+ and θ by ϕ in (10). In addition, the image of the lower and the upper boundaries by the axial symmetry, with axe the first bisector, represent the decision boundaries corresponding to $\frac{\pi}{2}-\phi$. A full illustration of 16-PSK is presented in Fig. 3.

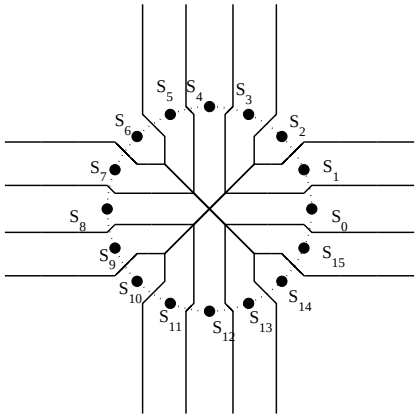

Fig. 3: Signal constellation and decision regions using the ML rule for 16-PSK.

As shown in the previous example (8-PSK), the construction of the decision boundaries in L_1 norm is complicated, especially for higher M $(16,32,64...)$ which of course leads to more complications in the SER calculation. However, the usual minimum euclidian distance presents a simple detector which leads to less complicated SER computations and final expressions.

D. Detection with L_2 Norm

When the receivers assume that the additional noise is Gaussian, while it is Laplacian in reality, the receiver uses the minimum euclidian distance detector instead of the L_1 norm detector. Therefore, it is necessary to study the behavior of the model presented above using the MD detector (L_2 norm detector) and compare the system performance of both detectors in presence of additive Laplacian noise.

To get the decision regions of an MPSK constellation using L_2 norm, we go back to (7) and replace the L_1 norm by the L_2 norm. In this one, decide ϕ if

$$|I-\cos(\phi)|^2+|Q-\sin(\phi)|^2<|I-\cos(\theta)|^2+|Q-\sin(\theta)|^2. \tag{11}$$

The decision region of ϕ lies in the part of the plan between the two angle $\phi-\frac{\pi}{M}$ and $\phi+\frac{\pi}{M}$. Fig.4 presents the detection zones for an example of 8-PSK. It is clear that these detection

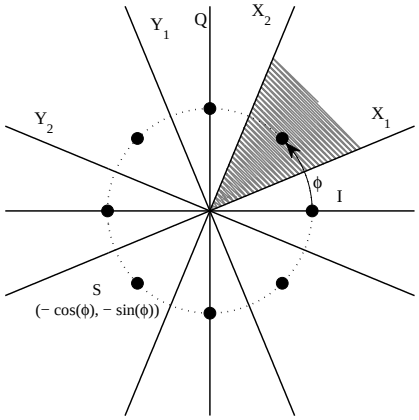

Fig. 4: Signal constellation and decision regions using the L_2 norm for 8-PSK.

zones are less complex than those presented in Fig.1. The axis (X_1,Y_1) and (X_2,Y_2) are a rotational transformation of (I,Q) and are studied in the next section.

III. Conditional Symbol Error Rate of M-PSK

In this section, we will compute the conditional SER using both detectors.

A. SER using the L_1 Norm Detector

1) SER of 8-PSK: From the general analysis given in subsection II-C and the decision boundaries presented in (9), the SER can be obtained from the probability of correct detection. In fact the probability of correct detection of ϕ can be evaluated as

$$\mathrm{P_c}(\phi|\gamma)=\int_{\text{Detection zone of }\phi} f_{IQ}(I,Q|\phi,\gamma)dIdQ. \tag{12}$$

Replace the detection zone and PDF of (I,Q), we get the probability of correct detection of each symbol. The total

This article has been accepted for publication in a future issue of this journal, but has not been fully edited. Content may change prior to final publication. Citation information: DOI 10.1109/TCOMM.2015.2438813, IEEE Transactions on Communications

probability of error can be obtained as

$$\begin{aligned}\Pr(e|\gamma) &= 1-\mathrm{P_c}(\gamma) = 1-\frac{1}{8}\sum_{k=0}^{7}\mathrm{P_c}\left(\frac{2k\pi}{8}\middle|\gamma\right)\\ &= \frac{1}{8}\left[4\left(2+(\sqrt{2}-1)\sqrt{2\gamma}\right)\mathrm{e}^{-\sqrt{\gamma}}\right.\\ &\quad\left.+\left(-1+(2-\sqrt{2})\sqrt{2\gamma}\right)\mathrm{e}^{-2\sqrt{\gamma}}\right].\end{aligned} \tag{13}$$

A generation of this result is developed in the next subsection.

2) SER of General M-PSK: To compute the SER for general MPSK constellation ($M \geq 8$), we proceed like in the previous special case by computing first the probability of correct detection and the probability of error of each symbol. The total SER is then obtained as the mean of all of the probability of error per symbol. As the decision regions are symmetric relative to the first bisector, we can limit our interest to the symbols with angles lie between 0 and $\frac{\pi}{4}$. The two limit cases, such that 0 and $\frac{\pi}{4}$, can be treated separately since their angle is known. The PDF of (I,Q) is defined by $f_{IQ}(I,Q) = \gamma e^{-2\sqrt{\gamma}(|I-1|+|Q|)}$ for $\phi = 0$. Hence, using the decision region presented in subsection II-C2, the probability of error of $\phi = 0$ can be evaluated as

$$\begin{aligned}P_e(0,\gamma) &= 1-2\gamma\left(\int_0^t\int_0^I e^{-2\sqrt{\gamma}(1-I+Q)}dQdI\right.\\ &\quad+\int_t^{\cos(\frac{2\pi}{M})}\int_0^t e^{-2\sqrt{\gamma}(1-I+Q)}dQdI\\ &\quad+\int_{\cos(\frac{2\pi}{M})}^1\int_0^{I+t-\cos(\frac{2\pi}{M})} e^{-2\sqrt{\gamma}(1-I+Q)}dQdI\\ &\quad\left.+\int_1^\infty\int_0^{t+1-\cos(\frac{2\pi}{M})} e^{-2\sqrt{\gamma}(I-1+Q)}dQdI\right),\end{aligned} \tag{14}$$

where $t = \frac{1}{2}\left(\cos(\frac{2\pi}{M})+\sin(\frac{2\pi}{M})-1\right)$.
In the same way, for $\phi = \frac{\pi}{4}$ the PDF of (I,Q) is defined by $f_{IQ}(I,Q) = \gamma e^{-2\sqrt{\gamma}\left(|I-\frac{\sqrt{2}}{2}|+|Q-\frac{\sqrt{2}}{2}|\right)}$. Thus the probability of error of $\phi = \frac{\pi}{4}$ can be expressed as

$$\begin{aligned}&P_e(\phi=\frac{\pi}{4},\gamma)\\ &= 1-\gamma\left(\int_{\frac{\sqrt{2}-u+v}{2}}^{\frac{\sqrt{2}}{2}}\int_{\frac{\sqrt{2}-u+v}{2}}^{\frac{\sqrt{2}}{2}} e^{2\sqrt{\gamma}\left(I+Q-\sqrt{2}\right)}dQdI\right.\\ &+\int_{\frac{\sqrt{2}-u+v}{2}}^{\frac{u+v}{2}}\int_{\frac{\sqrt{2}}{2}}^{I+\frac{u-v}{2}} e^{2\sqrt{\gamma}(I-Q)}dQdI\\ &+\int_{\frac{u+v}{2}}^{\frac{\sqrt{2}}{2}}\int_{\frac{\sqrt{2}}{2}}^{+\infty} e^{2\sqrt{\gamma}(I-Q)}dQdI+\int_{\frac{\sqrt{2}}{2}}^{u}\int_{I+\frac{v-u}{2}}^{\frac{\sqrt{2}}{2}} e^{2\sqrt{\gamma}(Q-I)}dQdI\\ &+\int_{u}^{+\infty}\int_{\frac{u+v}{2}}^{\frac{\sqrt{2}}{2}} e^{2\sqrt{\gamma}(Q-I)}dQdI\\ &\left.+\int_{\frac{\sqrt{2}}{2}}^{+\infty}\int_{\frac{\sqrt{2}}{2}}^{+\infty} e^{-2\sqrt{\gamma}(I+Q)-\sqrt{2}}dQdI\right),\end{aligned} \tag{15}$$

where $u = \cos(\frac{\pi}{4}-\frac{2\pi}{M})$ and $v = \sin(\frac{\pi}{4}-\frac{2\pi}{M})$. Finally, evaluating the above integrals and using algebraic simplifications and trigonometric formulas, (14) and (15) can be simplified to

$$\begin{aligned}&P_e(0,\gamma) = \sqrt{2\gamma}\sin\left(\frac{\pi}{M}\right)\cos\left(\frac{\pi}{M}+\frac{\pi}{4}\right)\mathrm{e}^{-2\sqrt{\gamma}}\\ &+\left(1+2\sqrt{\gamma}\sin\left(\frac{\pi}{M}\right)^2\right)\mathrm{e}^{-2\sin(\frac{\pi}{M})\cos\left(\frac{\pi}{M}-\frac{\pi}{4}\right)\sqrt{2\gamma}}\\ &P_e\left(\tfrac{\pi}{4},\gamma\right) = -\frac{1}{4}\mathrm{e}^{-2\sin(\frac{2\pi}{M})\sqrt{2\gamma}}\\ &+\left(1+2\sqrt{\gamma}\sin\left(\frac{\pi}{M}\right)\cos\left(\frac{\pi}{M}+\frac{\pi}{4}\right)\right)\mathrm{e}^{-\sin(\frac{2\pi}{M})\sqrt{2\gamma}}.\end{aligned} \tag{16}$$

On the other hand, the probability of error of other symbols is more complicated. For a general symbol i.e. angle $\phi = \frac{2k\pi}{M}$, lies between $\frac{2(k-1)\pi}{M}$ and $\frac{2(k+1)\pi}{M}$ for $1 \leq k \leq \frac{M}{8}-1$, the probability of error can be expressed in terms of cosine and sine these angles. For that let us define the series $c_k = \cos(\frac{2k\pi}{M})$, and $s_k = \sin(\frac{2k\pi}{M})$. A simple integration of the PDF of the received signal (I,Q) over the decision region of ϕ gives the expression in (17).

By computing these integrals and making some algebraic and trigonometric operation, P_e can be written in a simpler closed form

$$\begin{aligned}&P_e(\tfrac{2k\pi}{M},\gamma)\\ &= \frac{1}{2}\left[\mathrm{e}^{-2p\cos\left((2k-1)\delta-\frac{\pi}{4}\right)\sqrt{2\gamma}}\left(1+2\sqrt{\gamma}p\sin\left((2k-1)\delta\right)\right)\right.\\ &\quad\left.+\mathrm{e}^{-2p\cos\left((2k+1)\delta-\frac{\pi}{4}\right)\sqrt{2\gamma}}\left(1+2\sqrt{\gamma}p\sin\left((2k+1)\delta\right)\right)\right]\\ &+\frac{1}{8}\left[\mathrm{e}^{-2\cos\left(2k\delta+\frac{\pi}{4}\right)\sqrt{2\gamma}}\left(1+4\sqrt{2\gamma}p\cos\left((2k+1)\delta+\frac{\pi}{4}\right)\right)\right.\\ &\quad\left.-\mathrm{e}^{-2\cos\left(2(k-1)\delta+\frac{\pi}{4}\right)\sqrt{2\gamma}}\right],\end{aligned} \tag{18}$$

where $\delta = \frac{\pi}{M}$ and $p = \sin(\delta)$.

Assembling those expressions, the total symbol error rate is the average of the probability of error of all symbols which can be written as

$$\Pr(e|\gamma)=\frac{4}{M}\left[P_e(0,\gamma)+2\sum_{k=1}^{\frac{M}{8}-1}P_e\left(2k\delta,\gamma\right)+P_e\left(\frac{\pi}{4},\gamma\right)\right]. \tag{19}$$

Note that the SER of the previous special case (8-PSK) is included in this generic expression and equal to

$$\Pr(e|\gamma) = \frac{1}{2}\left[P_e(0,\gamma)+P_e\left(\frac{\pi}{4},\gamma\right)\right]. \tag{20}$$

The expression given in (19) does not cover the special cases of QPSK (4-PSK) and BPSK (2-PSK) because the decision region analysis, presented above, is constructed for $M \geq 8$. These two cases are very simple to deal because the decision region using L_1 norm is the same as the decision region using L_2 norm. Therefore, the SER of these special cases are presented in the next subsection which focuses on the SER of M-PSK using the L_2 norm detector.

B. SER using the L_2 Norm Detector

The general analysis of the SER of MPSK constellation in Gaussian noise environment was presented in [20]. We use, in what follows, a similar analysis to compute the SER of MPSK in LN environments. Assume that $s = (s_I, s_Q) =$

This article has been accepted for publication in a future issue of this journal, but has not been fully edited. Content may change prior to final publication. Citation information: DOI 10.1109/TCOMM.2015.2438813, IEEE Transactions on Communications

$$
\begin{aligned}
P_e(\frac{2k\pi}{M},\gamma) &= \int_{\frac{c_k+s_k+s_{k-1}-c_{k-1}}{2}}^{s_k}\int_{\frac{c_k+s_k+s_{k-1}-c_{k-1}}{2}}^{I} e^{2\sqrt{\gamma}(I-c_k+Q-s_k)}dQdI \\
&+ \int_{s_k}^{c_k}\int_{\frac{c_k+s_k+s_{k-1}-c_{k-1}}{2}}^{s_k} e^{2\sqrt{\gamma}(I-c_k+Q-s_k)}dQdI + \int_{s_k}^{\frac{c_{k+1}+s_{k+1}+s_k-c_k}{2}}\int_{s_k}^{I} e^{2\sqrt{\gamma}(I-c_k-Q+s_k)}dQdI \\
&+ \int_{\frac{c_{k+1}+s_{k+1}+s_k-c_k}{2}}^{c_k}\int_{s_k}^{\frac{c_{k+1}+s_{k+1}+s_k-c_k}{2}} e^{2\sqrt{\gamma}(I-c_k-Q+s_k)}dQdI \\
&+ \int_{c_{k+1}}^{c_k}\int_{\frac{c_{k+1}+s_{k+1}+s_k-c_k}{2}}^{I+\frac{s_{k+1}-c_{k+1}+s_k-c_k}{2}} e^{2\sqrt{\gamma}(I-c_k-Q+s_k)}dQdI \int_{c_k}^{c_{k-1}}\int_{I+\frac{s_k-c_k+s_{k-1}-c_{k-1}}{2}}^{\frac{s_k-c_k+s_{k-1}+c_{k-1}}{2}} e^{2\sqrt{\gamma}(-I+c_k+Q-s_k)}dQdI \\
&+ \int_{c_k}^{+\infty}\int_{\frac{s_k-c_k+s_{k-1}+c_{k-1}}{2}}^{s_k} e^{2\sqrt{\gamma}(-I+c_k+Q-s_k)}dQdI + \int_{c_k}^{+\infty}\int_{s_k}^{\frac{c_k+s_k+s_{k+1}-c_{k+1}}{2}} e^{2\sqrt{\gamma}(-I+c_k-Q+s_k)}dQdI
\end{aligned} \tag{17}
$$

$(-\cos(\phi),-\sin(\phi))$ is sent. The objective is to compute the probability of error detection of s for general ϕ. To do so, consider two rotations of coordinates, i.e. rotation transformation from (I,Q) to (X_1,Y_1) with rotation angle $\phi-\theta$, and from (I,Q) to (X_2,Y_2) with rotation angle $\phi+\theta$ (see Fig.4). Using two transformation matrices, we get the new basis from the initial basis as

$$
\begin{bmatrix} X_1 \\ Y_1 \end{bmatrix} = \begin{bmatrix} \cos(\phi-\theta) & \sin(\phi-\theta) \\ -\sin(\phi-\theta) & \cos(\phi-\theta) \end{bmatrix} \begin{bmatrix} I \\ Q \end{bmatrix}, \tag{21}
$$

and

$$
\begin{bmatrix} X_2 \\ Y_2 \end{bmatrix} = \begin{bmatrix} \cos(\phi+\theta) & \sin(\phi+\theta) \\ -\sin(\phi+\theta) & \cos(\phi+\theta) \end{bmatrix} \begin{bmatrix} I \\ Q \end{bmatrix}. \tag{22}
$$

From Fig.4, the SER can be expressed as

$$
Pe(\gamma,\phi) = \Pr(Y_1 \geq 0) + \Pr(Y_2 \leq 0) - \Pr(Y_1 \geq 0, Y_2 \leq 0). \tag{23}
$$

Thus, to compute the SER for MPSK, we have to find the PDF of Y_1 and Y_2 separately and also their joint PDF. From (21) and (22), Y_1 and Y_2 appear as the sum of two independent Laplacian random variables with means $E[Y_1] = -\sin\theta$, $E[Y_2] = \sin\theta$, and variances $\sigma^2_{Y_1} = \sigma^2_{Y_2} = \frac{1}{2\gamma}$.

Let us consider two independent Laplacian random variables $(Z_1,Z_2) \sim (\mathcal{L}(0,\sigma_1),\mathcal{L}(0,\sigma_2))$, and suppose $Y = Z_1 + Z_2$. The PDF of Y is given in [26, Eq. (3.3.23)] as

$$
f_Y(y) = \begin{cases} \frac{1}{2\sigma}\left(\frac{1}{\sqrt{2}} + \frac{|y|}{\sigma}\right)e^{-\sqrt{2}\frac{|y|}{\sigma}} & \text{if } \sigma = \sigma_1 = \sigma_2 \\ \frac{1}{\sqrt{2}(\sigma_1^2-\sigma_2^2)}\left(\sigma_1 e^{-\sqrt{2}\frac{|y|}{\sigma_1}} - \sigma_2 e^{-\sqrt{2}\frac{|y|}{\sigma_2}}\right) & \text{if } \sigma_1 \neq \sigma_2. \end{cases} \tag{24}
$$

This property can be extended to the non zero mean case by a centralization of the random variable $Y' = Y - E[Y]$. Consequently, the PDF of Y_1 and Y_2 can be obtained as follows

$$
\begin{aligned}
f_{Y_1}(y) &= \frac{\sqrt{\gamma}}{\cos 2(\phi-\theta)}\left(|\cos(\phi-\theta)|e^{-\frac{2\sqrt{\gamma}|y+sin\theta|}{|\cos(\phi-\theta)|}} - |\sin(\phi-\theta)|e^{-\frac{2\sqrt{\gamma}|y+sin\theta|}{|\sin(\phi-\theta)|}}\right) \\
f_{Y_2}(y) &= \frac{\sqrt{\gamma}}{\cos 2(\phi+\theta)}\left(|\cos(\phi+\theta)|e^{-\frac{2\sqrt{\gamma}|y-sin\theta|}{|\cos(\phi+\theta)|}} - |\sin(\phi+\theta)|e^{-\frac{2\sqrt{\gamma}|y-sin\theta|}{|\sin(\phi+\theta)|}}\right).
\end{aligned} \tag{25}
$$

Using (24), the probabilities $\Pr(Y_1 \geq 0)$ and $\Pr(Y_2 \leq 0)$ in (23) can easily be obtained as

$$
\begin{aligned}
\Pr(Y_1 \geq 0) &= \int_0^\infty f_{Y_1}(y_1)dy_1 \\
&= \frac{1}{2\cos 2(\phi-\theta)}\left(\cos^2(\phi-\theta)e^{\frac{-2\sin\theta}{|\cos(\phi-\theta)|}\sqrt{\gamma}} - \sin^2(\phi-\theta)e^{\frac{-2\sin\theta}{|\sin(\phi-\theta)|}\sqrt{\gamma}}\right)
\end{aligned} \tag{26}
$$

$$
\begin{aligned}
\Pr(Y_2 \leq 0) &= \int_{-\infty}^0 f_{Y_2}(y_2)dy_2 \\
&= \frac{1}{2\cos 2(\phi+\theta)}\left(\cos^2(\phi+\theta)e^{\frac{-2\sin\theta}{|\cos(\phi+\theta)|}\sqrt{\gamma}} - \sin^2(\phi+\theta)e^{\frac{-2\sin\theta}{|\sin(\phi+\theta)|}\sqrt{\gamma}}\right).
\end{aligned} \tag{27}
$$

Now, we have to evaluate the probability $\Pr(Y_1 \geq 0, Y_2 \leq 0)$ in (23) and this represents the probability of the shaded region in Fig.4. First we have to find the joint PDF of (Y_1,Y_2). From (21) and (22), (Y_1,Y_2) can be written as a linear transformation of (I,Q) as

$$
\begin{bmatrix} Y_1 \\ Y_2 \end{bmatrix} = \begin{bmatrix} -\sin(\phi-\theta) & \cos(\phi-\theta) \\ -\sin(\phi+\theta) & \cos(\phi+\theta) \end{bmatrix} \begin{bmatrix} I \\ Q \end{bmatrix} = A \begin{bmatrix} I \\ Q \end{bmatrix}. \tag{28}
$$

Using this change of variable, the joint PDF of (Y_1,Y_2) can be obtained from the joint PDF of (I,Q) (6) using the transformation formula

$$
\begin{aligned}
f_{Y_1Y_2}(y_1,y_2) &= \frac{1}{\det(A)} f_{IQ}(A^{-1}[y_1,y_2]^T) \\
&= \frac{\gamma}{\sin 2\theta} e^{-\frac{2\sqrt{\gamma}}{\sin 2\theta}T},
\end{aligned} \tag{29}
$$

where

$$
\begin{aligned}
T &= |\cos(\phi+\theta)(y_1+\sin\theta) - \cos(\phi-\theta)(y_2-\sin\theta)| \\
&+ |\sin(\phi+\theta)(y_1+\sin\theta) - \sin(\phi-\theta)(y_2-\sin\theta)|
\end{aligned}
$$

Once we obtain $f_{Y_1Y_2(y_1,y_2)}$, the probability $\Pr(Y_1 \geq 0, Y_2 \leq 0)$ can easily be obtained as

$$
\begin{aligned}
\Pr(Y_1 \geq 0, Y_2 \leq 0) &= \int_0^\infty \int_{-\infty}^0 f_{Y_1Y_2}(y_1,y_2)dy_2dy_1 \\
&= \begin{cases} \frac{\sin\theta}{2(\cos\theta+\sin\theta)}e^{-2\sqrt{\gamma}} \text{ if } \phi = 0 \\ \frac{\sin 2\theta}{4(\cos 2\theta+\sin 2\phi)}e^{-2\sqrt{\gamma}(\cos\phi+\sin\phi)} \text{ if } \phi > 0. \end{cases}
\end{aligned} \tag{30}
$$

This article has been accepted for publication in a future issue of this journal, but has not been fully edited. Content may change prior to final publication. Citation information: DOI 10.1109/TCOMM.2015.2438813, IEEE Transactions on Communications

At this point, by substituting (26),(27), and (30) into (23), we get the probability of error of $s = (-\cos\phi, -\sin\phi)$ for general $\phi \in [0, \frac{\pi}{2}[$, $Pe(\gamma, \phi)$

$$\begin{cases} Pe\,(\gamma,0) & = \frac{1}{1-\tan(\theta)^2} e^{-\tan(\theta)\sqrt{2\gamma}} - \frac{\tan(\theta)}{2(1-\tan(\theta))} e^{-\sqrt{2\gamma}} \\ Pe\,(\gamma,\phi) & = \frac{1}{2\cos 2(\phi-\theta)} \left(\cos^2(\phi-\theta) e^{\frac{-2\sin\theta}{\cos(\phi-\theta)}\sqrt{\gamma}} \right. \\ & \quad \left. - \sin^2(\phi-\theta) e^{\frac{-2\sin\theta}{\sin(\phi-\theta)}\sqrt{\gamma}} \right) \\ & \quad + \frac{1}{2\cos 2(\phi+\theta)} \left(\cos^2(\phi+\theta) e^{\frac{-2\sin\theta}{\cos(\phi+\theta)}\sqrt{\gamma}} \right. \\ & \quad \left. - \sin^2(\phi+\theta) e^{\frac{-2\sin\theta}{\sin(\phi+\theta)}\sqrt{\gamma}} \right) \\ & \quad - \frac{\sin 2\theta}{4(\cos 2\theta + \sin 2\phi)} e^{-2(\cos\phi+\sin\phi)\sqrt{\gamma}}. \end{cases} \tag{31}$$

As the symbols are equiprobable and distributed uniformly on the unit circle and from the symmetric properties of the PDF of Laplacian random variable, we can limit ourselves to the symbols lying between 0 and $\frac{\pi}{2}$ so $0 \le \phi < \frac{\pi}{2}$. In addition, ϕ can take the values $\phi = \frac{2k\pi}{M}$, for $k = 0, 1 \ldots \frac{M}{4} - 1$, and the total SER can be expressed as

$$\Pr(e|\gamma) = \frac{4}{M} \sum_{k=0}^{\frac{M}{4}-1} Pe\left(\gamma, \frac{2k\pi}{M}\right). \tag{32}$$

Finally, combining (31) and (32) with $\theta = \pi/M = \delta$, and using some algebraic simplifications, it can be shown that the general closed-form expression for the conditional SER of MPSK over LN using the L_2 norm detector, $\Pr(e|\gamma)$, can be expressed as

$$\Pr(e|\gamma) = \frac{8}{M} \sum_{k=0}^{\frac{M}{4}-1} g(k,\gamma) + \frac{2\tan(\delta)^2 e^{-2\sqrt{\gamma}}}{M(1-\tan(\delta)^2)}, \tag{33}$$

where

$$\begin{aligned} g(k,\gamma) = & \frac{1}{2\cos\left(2(2k+1)\delta\right)} \left(\cos\left((2k+1)\delta\right)^2 e^{\frac{-2p\sqrt{\gamma}}{\cos((2k+1)\delta)}} \right. \\ & \left. - \sin\left((2k+1)\delta\right)^2 e^{\frac{-2p\sqrt{\gamma}}{\sin((2k+1)\delta)}} \right) \\ & - \frac{\sin(2\delta)}{8\left(\cos(2\delta)+\sin(4k\delta)\right)} e^{-2\sqrt{2}\cos\left(2k\delta-\frac{\pi}{4}\right)\sqrt{\gamma}}. \end{aligned} \tag{34}$$

This expression is valid for $M \ge 8$. The special case of $M = 4$, appears as a limit of this expression and the SER can be expressed in this case as

$$\Pr(e|\gamma) = \left(\frac{3}{4} + \sqrt{\gamma}\right) e^{-2\sqrt{\gamma}}. \tag{35}$$

For $M = 2$, the conditional SER can be evaluated from the original expression (23) as

$$\Pr(e|\gamma) = \frac{1}{2} e^{-2\sqrt{\gamma}}, \tag{36}$$

which is the same result found in [27, Eq. (12)]. Note, as mentioned at the end of subsection III-A2, that the results in (35) and (36) are the same using L_2 or L_1 norm. They will be treated as special cases in the following section since they can not be included in the generic formula.

Let us focus now on the case of $M \ge 8$. Using some of the properties of $g(k,\gamma)$ (33) can be further simplified and written compactly as

$$\begin{aligned} \Pr(e|\gamma) = & \frac{16}{M} \sum_{k=0}^{\frac{M}{8}-1} g(k,\gamma) \\ & - \frac{1}{M} \tan\left(\frac{\pi}{M}\right) \left(e^{-2\sqrt{2\gamma}} - \frac{2}{1-\tan(\frac{\pi}{M})} e^{-2\sqrt{\gamma}} \right). \end{aligned} \tag{37}$$

Proof: $g(k,\gamma)$ has the following property

$$\begin{aligned} & g(\tfrac{M}{4} - k - 1, \gamma) = g(k,\gamma) \\ & + \sin(2\delta) \left(\frac{e^{-2\sqrt{2}\cos\left(2k\delta-\frac{\pi}{4}\right)\sqrt{\gamma}}}{8(\cos(2\delta)+\sin(4k\delta))} - \frac{e^{-2\sqrt{2}\cos\left(2(k+1)\delta-\frac{\pi}{4}\right)\sqrt{\gamma}}}{8(\cos(2\delta)+\sin(4(k+1)\delta))} \right), \end{aligned} \tag{38}$$

Thus the sum of $g(k,\gamma)$ can be simplified as follows

$$\begin{aligned} & \sum_{k=0}^{\frac{M}{4}-1} g(k,\gamma) \\ & = \sum_{k=0}^{\frac{M}{8}-1} g(k,\gamma) + \sum_{k=\frac{M}{8}}^{\frac{M}{4}-1} g(k,\gamma) \\ & = \sum_{k=0}^{\frac{M}{8}-1} g(k,\gamma) + \sum_{l=0}^{\frac{M}{8}-1} g(\frac{M}{4} - l - 1, \gamma) \\ & = 2 \sum_{k=0}^{\frac{M}{8}-1} g(k,\gamma) + \sin(2\delta) \\ & \times \textstyle\sum_{k=0}^{\frac{M}{8}-1} \left(\frac{e^{-2\sqrt{2}\cos\left(2k\delta-\frac{\pi}{4}\right)\sqrt{\gamma}}}{8(\cos(2\delta)+\sin(4k\delta))} - \frac{e^{-2\sqrt{2}\cos\left(2(k+1)\delta-\frac{\pi}{4}\right)\sqrt{\gamma}}}{8(\cos(2\delta)+\sin(4(k+1)\delta))} \right) \\ & = 2 \sum_{k=0}^{\frac{M}{8}-1} g(k,\gamma) + \sin(2\delta) \\ & \times \left(\textstyle\sum_{k=0}^{\frac{M}{8}-1} \frac{e^{-2\sqrt{2}\cos\left(2k\delta-\frac{\pi}{4}\right)\sqrt{\gamma}}}{8(\cos(2\delta)+\sin(4k\delta))} - \sum_{k=1}^{\frac{M}{8}} \frac{e^{-2\sqrt{2}\cos\left(2k\delta-\frac{\pi}{4}\right)\sqrt{\gamma}}}{8(\cos(2\delta)+\sin(4k\delta))} \right) \\ & = 2 \sum_{k=0}^{\frac{M}{8}-1} g(k,\gamma) + \frac{\tan(2\delta)}{8} e^{-2\sqrt{\gamma}} - \frac{\sin(2\delta)}{8(\cos(2\delta)+1)} e^{-2\sqrt{2\gamma}}. \end{aligned} \tag{39}$$

■

C. Comparison between the SER using the L_1 Norm and the L_2 Norm Detectors

In Fig. 5 we draw the conditional SER for different size of constellation versus the instantaneous SNR for the ML detector and the MD detector. From the curves it is clear that the system performance degrades by increasing the constellation size M. Moreover, as mentioned before, the results in the QPSK case are the same using the L_1 norm or the L_2 norm detectors. For $M \ge 8$, the difference between the SER of both detectors is small with an advantage to the L_1 norm (solid lines), ML detector, as expected. In addition, it should be noted that by increasing M, the SNR gap for a fixed SER between the two detectors becomes smaller (from 0.6 dB for 8-PSK to 0.2 dB for 64-PSK at SER= 10^{-5}). To explain this fact, Fig. 6 represents the intersection zones between the decision regions created by ML and MD detectors for 8-PSK (these zones are colored in black). From the figure, note that the area of different decisions between the two detectors is very low compared to the remaining surface, which explains

This article has been accepted for publication in a future issue of this journal, but has not been fully edited. Content may change prior to final publication. Citation information: DOI 10.1109/TCOMM.2015.2438813, IEEE Transactions on Communications

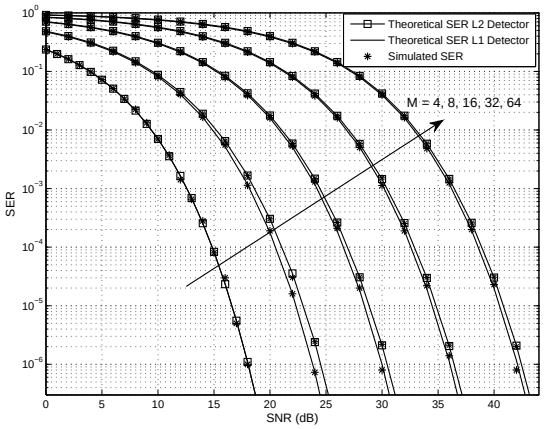

Fig. 5: Difference between the L_1 norm and L_2 norm detectors in an AWLN channel (stars denote the simulation results for both detectors).

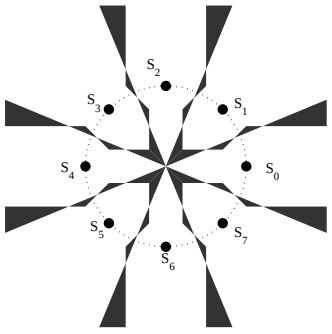

Fig. 6: Intersection between decision regions created by the ML and MD detectors for 8-PSK.

why the performance gap is small. As a consequence of these results, the use of L_2 norm in detection of signals subject to AWLN, by wrong assumptions of the noise distribution or simplification of detector, does not affect harmfully the performance of the system especially for higher size of the constellation. In the next section, we include the fading in our model to quantify the impact of such attenuation on the performance of MPSK in presence of additive LN.

IV. Average Symbol Error Rate of M-PSK

All the analysis presented above are conditioned on the fading coefficient, and are as such function of the instantaneous SNR. In the presence of slow fading, the ASER can be obtained by averaging the SER issued from both detectors, (19) and (33), over the PDF of the SNR γ, $p_\gamma(\gamma)$, yielding

$$\Pr(e) = \int_0^\infty \Pr(e|\gamma) p_\gamma(\gamma)\, d\gamma. \tag{40}$$

Two types of integrals appear in the evaluations of the ASER, while the first integral, called $\mathcal{I}(x)$, considers an integral of the product of the PDF of γ, $p_\gamma(\gamma)$, and an exponential, the second integral, named $\mathcal{J}(x)$, consist of an integral of the product of the PDF of γ, an exponential function, and square root of γ. More specifically, they are defined as

$$\mathcal{I}(x) = \int_0^\infty p_\gamma(\gamma) e^{-x\sqrt{\gamma}}\, d\gamma, \quad \forall\ x \geq 0 \tag{41}$$

$$\mathcal{J}(x) = \int_0^\infty \sqrt{\gamma} p_\gamma(\gamma) e^{-x\sqrt{\gamma}}\, d\gamma = -\mathcal{I}'(x),\ \forall\ x \geq 0. \tag{42}$$

By derivation of $\mathcal{I}$ with respect to x, we can get easily $\mathcal{J}$ which is the opposite of the derivative of $\mathcal{I}$, namely $\mathcal{I}'$. Therefore, the ASER of the MPSK system, computed by L_1 norm or L_2 norm techniques, is expressed in terms of the functions $\mathcal{I}$ and $\mathcal{I}'$ in the next analysis.

The ASER of MPSK constellation using the ML detector can be deduced from the general conditional expression (19) and the averaging formula (40), the final ASER expression, for $M \geq 8$, can be presented as

$$\begin{aligned}\Pr_{ML}(e) = \frac{1}{M}\sum_{k=1}^{\frac{M}{8}-1} F(k) - \frac{1}{M}\mathcal{I}\left(2\sqrt{2}\sin(2\delta)\right) \\ +\frac{4}{M}\Big[\mathcal{I}\left(2\sqrt{2}p\cos\left(\delta-\frac{\pi}{4}\right)\right) - 2p^2\mathcal{I}'\left(2\sqrt{2}p\cos\left(\delta-\frac{\pi}{4}\right)\right) \\ -\sqrt{2}p\cos\left(\delta+\frac{\pi}{4}\right)\mathcal{I}'(2) + \mathcal{I}\left(\sqrt{2}\sin(2\delta)\right) \\ -2p\cos\left(\delta+\tfrac{\pi}{4}\right)\mathcal{I}'\left(\sqrt{2}\sin(2\delta)\right)\Big],\end{aligned} \tag{43}$$

where the generic function $F(k)$ is expressed as

$$\begin{aligned}F(k) = 4\mathcal{I}\left(2\sqrt{2}p\cos\left((2k-1)\delta-\frac{\pi}{4}\right)\right) \\ -8p\sin\left((2k-1)\delta\right)\mathcal{I}'\left(2\sqrt{2}p\cos\left((2k-1)\delta-\frac{\pi}{4}\right)\right) \\ -8p\sin\left((2k+1)\delta\right)\mathcal{I}'\left(2\sqrt{2}p\cos\left((2k+1)\delta-\frac{\pi}{4}\right)\right) \\ -4\sqrt{2}p\cos\left((2k+1)\delta+\frac{\pi}{4}\right)\mathcal{I}'\left(2\sqrt{2}\cos\left(2k\delta+\frac{\pi}{4}\right)\right) \\ +4\mathcal{I}\left(2\sqrt{2}p\cos\left((2k+1)\delta-\frac{\pi}{4}\right)\right) \\ -\mathcal{I}\left(2\sqrt{2}\cos\left(2(k-1)\delta+\frac{\pi}{4}\right)\right) \\ +\mathcal{I}\left(2\sqrt{2}\cos\left(2k\delta+\frac{\pi}{4}\right)\right).\end{aligned} \tag{44}$$

Using the same method to compute the average probability of error, the ASER of MPSK constellation using MD detector can be expressed, for $M \geq 8$, as

$$\Pr_{MD}(e) = \frac{8}{M}\sum_{k=0}^{\frac{M}{4}-1} G(k) + \frac{2\tan(\frac{\pi}{M})^2}{M(1-\tan(\frac{\pi}{M})^2)}\mathcal{I}(2), \tag{45}$$

where

$$\begin{aligned}G(k) = \frac{1}{2\cos(2k+1)\frac{2\pi}{M}}\left(\cos\left((2k+1)\tfrac{\pi}{M}\right)^2\mathcal{I}\left(\frac{2\sin(\frac{\pi}{M})}{\cos\left((2k+1)\frac{\pi}{M}\right)}\right)\right. \\ \left. -\sin\left((2k+1)\tfrac{\pi}{M}\right)^2\mathcal{I}\left(\frac{2\sin(\frac{\pi}{M})}{\sin\left((2k+1)\frac{\pi}{M}\right)}\right)\right) \\ -\frac{\sin(\frac{2\pi}{M})}{8\left(\cos(\frac{2\pi}{M})+\sin(\frac{4k\pi}{M})\right)}\mathcal{I}\left(2\sqrt{2}\cos\left(\tfrac{2k\pi}{M}-\tfrac{\pi}{4}\right)\right).\end{aligned} \tag{46}$$

As mentioned above, this expression is actually valid for $M \geq 4$, since the $M = 4$ case appears as a limit case. In particular, from (35), the ASER of QPSK with ML and MD detector can be evaluated as

$$\Pr_{QPSK}(e) = \frac{3}{4}\mathcal{I}(2) - \mathcal{I}'(2). \tag{47}$$

This article has been accepted for publication in a future issue of this journal, but has not been fully edited. Content may change prior to final publication. Citation information: DOI 10.1109/TCOMM.2015.2438813, IEEE Transactions on Communications

Finally, for $M = 2$, from (36) the ASER is equal to $\Pr_{BPSK}(e) = \mathcal{I}(2)/2$.

The major remark from the previous analysis is that the ASER, using ML and MD detectors, is fully defined by knowing $\mathcal{I}(x)$ and $\mathcal{I}'(x)$ for the desired type of fading. Consequently, we are focusing on the next subsections on the evaluation of $\mathcal{I}$ and $\mathcal{I}'$ for a generic type of fading, namely the EGK distribution, from which we can extract many common fading distributions.

A. EGK Fading

The fading envelope $\mathcal{H}$ is assumed to follow a very general fading distribution, namely, the EGK distribution. This distribution captures many common fading distributions as special cases, like Rayleigh fading, Nakagami-m fading, K distribution and many other distributions summarized in [24].

From the definition of the instantaneous SNR, γ, derived from the channel envelope $\mathcal{H}$, the PDF of γ with average $\overline{\gamma} = \mathbb{E}[\gamma]$, can be given as [23, Eq. (2)]

$$p_\gamma(\gamma) = \frac{\xi}{\Gamma(m_s)\Gamma(m)} \left(\frac{\beta_s \beta}{\overline{\gamma}}\right)^{m\xi} \gamma^{m\xi-1} \times \Gamma\left(m_s - m\frac{\xi}{\xi_s}, 0, \left(\frac{\beta_s\beta}{\overline{\gamma}}\right)^{\xi}\gamma^{\xi}, \frac{\xi}{\xi_s}\right), \quad (48)$$

defined over $\gamma \in (0, \infty)$. In (48), the parameters m ($0.5 \leq m < \infty$) and ξ ($0 \leq \xi < \infty$) represent the fading figure (diversity severity / order) and the fading shaping factor, respectively, while m_s ($0.5 \leq m_s < \infty$) and ξ_s ($0 \leq \xi_s < \infty$) represent the shadowing severity and the shadowing shaping factor (inhomogeneity), respectively. Furthermore, $\Gamma(.)$ is the Gamma function, the parameters $\beta = \Gamma(m + 1/\xi)/\Gamma(m)$, $\beta_s = \Gamma(m_s + 1/\xi_s)/\Gamma(m_s)$, and $\Gamma(\cdot,\cdot,\cdot,\cdot)$ is the extended incomplete Gamma function defined in [28, Eq. (6.2)] as

$$\Gamma(a, x, b, \beta) = \int_x^\infty r^{a-1} \exp\left(-r - br^{-\beta}\right) dr, \quad (49)$$

where $a, \beta, b \in \mathbb{C}$ and $x \in \mathbb{R}^+$.

An alternative expression of $p_\gamma(\gamma)$ in terms of the Fox H function (FHF) [29, Eq. (1.1.1)], [30], $\mathrm{H}[.]$, is useful in this section to compute the average SER. An efficient implementation of the FHF on MATHEMATICA® is given in [31, Appendix]. Moreover, $p_\gamma(\gamma)$ can be re-written as

$$p_\gamma(\gamma) = \frac{1}{\Gamma(m_s)\Gamma(m)\gamma} \mathrm{H}_{0,2}^{2,0}\left[\frac{\beta_s\beta}{\overline{\gamma}}\gamma \middle| \overline{\begin{matrix}\\ (m_s, \frac{1}{\xi_s}), (m, \frac{1}{\xi})\end{matrix}}\right]. \quad (50)$$

Substitute the alternative expression of $p_\gamma(\gamma)$ in $\mathcal{I}(x)$, use the representation of the exponent in terms of the FHF [29, Eq. (2.9.4)], $e^x = \mathrm{H}_{0,1}^{1,0}\left[-x \middle| \overline{\begin{matrix}\\ (0,1)\end{matrix}}\right]$, and use the identity [29, Eq. (2.8.4)] that computes an integral of two FHF, the integral function $\mathcal{I}(x)$ can be expressed in terms of the FHF as

$$\begin{aligned}\mathcal{I}(x) &= \frac{1}{\Gamma(m_s)\Gamma(m)} \int_0^\infty \frac{1}{\gamma} e^{-x\sqrt{\gamma}} \mathrm{H}_{0,2}^{2,0}\left[\frac{\beta_s\beta}{\overline{\gamma}}\gamma \middle| \overline{\begin{matrix}\\ (m_s, \frac{1}{\xi_s}), (m, \frac{1}{\xi})\end{matrix}}\right] d\gamma \\ &= \frac{2}{\Gamma(m_s)\Gamma(m)} \mathrm{H}_{1,2}^{2,1}\left[\frac{\beta_s\beta}{\overline{\gamma}x^2} \middle| \begin{matrix}(1,2)\\ (m_s, \frac{1}{\xi_s}), (m, \frac{1}{\xi})\end{matrix}\right]. \quad (51)\end{aligned}$$

The identity [29, Eq. (2.2.1)] gives the derivative of the FHF, that is used to computed $\mathcal{I}'$ and which is equal to

$$\mathcal{I}'(x) = \frac{-2}{x\Gamma(m_s)\Gamma(m)} \mathrm{H}_{1,2}^{2,1}\left[\frac{\beta_s\beta}{\overline{\gamma}x^2} \middle| \begin{matrix}(0,2)\\ (m_s, \frac{1}{\xi_s}), (m, \frac{1}{\xi})\end{matrix}\right]. \quad (52)$$

The results given in (51) and (52) are valid for the general EGK fading scenario. In the next subsections, we simplify these results for some useful special cases such as the Generalized-K, Generalized Nakagami-m, Nakagami-m, and Rayleigh fading distributions.

B. Generalized-K Fading

The generalized-K (GK) fading is obtained by setting $\xi = 1$ and $\xi_s = 1$ in the parameters of the EGK distribution (48), and in this case m and m_s become the parameters of the GK distribution. By replacing ξ and ξ_s by their value in (51), $\mathcal{I}$ can be re-written as

$$\mathcal{I}(x) = \frac{2}{\Gamma(m_s)\Gamma(m)} \mathrm{H}_{1,2}^{2,1}\left[\frac{mm_s}{\overline{\gamma}x^2} \middle| \begin{matrix}(1,2)\\ (m_s,1), (m,1)\end{matrix}\right]. \quad (53)$$

Using the simplification made in [32, Table IV], $\mathcal{I}$ can be expressed in terms of the standard Meijer G-function (MGF) [29, Eq. (2.9.1)] as

$$\mathcal{I}(x) = \frac{1}{\Gamma(m_s)\Gamma(m)\sqrt{\pi}} \mathrm{G}_{2,2}^{2,2}\left[\frac{4mm_s}{\overline{\gamma}x^2} \middle| \begin{matrix}1, 1/2\\ m, m_s\end{matrix}\right]. \quad (54)$$

Using the derivative properties of the MGF, $\mathcal{I}'$ is evaluated as

$$\mathcal{I}'(x) = \frac{-2}{x\Gamma(m_s)\Gamma(m)\sqrt{\pi}} \mathrm{G}_{2,2}^{2,2}\left[\frac{4mm_s}{\overline{\gamma}x^2} \middle| \begin{matrix}0, 1/2\\ m, m_s\end{matrix}\right] \quad (55)$$

These final expressions in terms of the MGF are less complex than the expressions in terms of the FHF, since the MGF is already a built-in function in standard mathematical packages such as MATHEMATICA®.

C. Generalized Nakagami-m Fading

This type of fading is obtained by setting the quadruplet (m, ξ, m_s, ξ_s) to $(m, \xi, \infty, 1)$ in (51). Using the limit property given in [27, Eq. (B.1)] and the inverse Mellin transform of the extended incomplete Gamma function $\Gamma(.,.;.;.)$ [28, Eq. (6.29)], one can show that

$$\begin{aligned}\mathcal{I}(x) &= \frac{2}{\Gamma(m)} \mathrm{H}_{1,1}^{1,1}\left[\frac{\beta}{\overline{\gamma}x^2} \middle| \begin{matrix}(1,2)\\ (m, \frac{1}{\xi})\end{matrix}\right] \\ &= \frac{2\xi}{\Gamma(m)} \left(\frac{\beta}{x^2\overline{\gamma}}\right)^{m\xi} \Gamma\left(2m\xi, 0; \left(\frac{\beta}{x^2\overline{\gamma}}\right)^{\xi}; -2\xi\right). \quad (56)\end{aligned}$$

This article has been accepted for publication in a future issue of this journal, but has not been fully edited. Content may change prior to final publication. Citation information: DOI 10.1109/TCOMM.2015.2438813, IEEE Transactions on Communications

A similar expression of $\mathcal{I}'$ is obtained using the derivative expression of the FHF and the Mellin transform of the extended incomplete Gamma function, its closed form is evaluated as

$$\mathcal{I}'(x) = \frac{-2\xi}{x\Gamma(m)} \left(\frac{\beta}{x^2\overline{\gamma}}\right)^{m\xi} \Gamma\left(1+2m\xi, 0; \left(\frac{\beta}{x^2\overline{\gamma}}\right)^{\xi}; -2\xi\right). \tag{57}$$

D. Nakagami-m Fading

From the previous case, the Nakagami-m fading may be obtained by replacing ξ by 1. By using the special case of the extended incomplete Gamma function [28, Eq. (6.44)], $\mathcal{I}$ can be expressed as

$$\begin{aligned} \mathcal{I}(x) &= \frac{2}{\Gamma(m)} \left(\frac{m}{x^2\overline{\gamma}}\right)^{m} \Gamma(2m, 0; \frac{m}{x^2\overline{\gamma}}; -2) \\ &= \frac{2\Gamma(2m)}{4^m\Gamma(m)} U\left(m, \frac{1}{2}, \frac{\overline{\gamma}x^2}{4m}\right), \end{aligned} \tag{58}$$

where $U(.,.,.)$ is the Tricomi confluent hypergeometric function [33, Chapter 13]. Using the derivative of the $U(.,.,.)$ function [33, Eq. (13.4.21)], we get $\mathcal{I}'$ as

$$\mathcal{I}'(x) = -\frac{\Gamma(2m)\overline{\gamma}x}{4^m\Gamma(m)} U\left(m+1, \frac{3}{2}, \frac{\overline{\gamma}x^2}{4m}\right). \tag{59}$$

E. Rayleigh Fading

The Rayleigh fading is one of the basic fading models, and is a special case of the Nakagami-m fading be setting $m = 1$. Using the special cases of the Hypergeometric function, and an integration by parts, the principal function $\mathcal{I}$ may be simplified in this case to

$$\begin{aligned} \mathcal{I}(x) &= \frac{1}{2} U\left(2, \frac{1}{2}, \frac{\overline{\gamma}x^2}{4}\right) = \frac{1}{4}\sqrt{\overline{\gamma}x^2} e^{\frac{\overline{\gamma}x^2}{4}} \Gamma\left(-\frac{1}{2}, \frac{\overline{\gamma}x^2}{4}\right) \\ &= 1 - \sqrt{\overline{\gamma}x^2\pi} e^{\frac{\overline{\gamma}x^2}{4}} Q\left(\sqrt{\frac{\overline{\gamma}x^2}{2}}\right), \end{aligned} \tag{60}$$

where $\Gamma(.,.)$ is the incomplete Gamma function, and Q is the standard Gaussian Q function [27, Eq. (A.1)].

Also the derivative of $\mathcal{I}$ can be obtained easily by taking the derivative of the Q function yielding

$$\mathcal{I}'(x) = \frac{1}{2}\overline{\gamma}x - \frac{1}{2}(2+\overline{\gamma}x^2)\sqrt{\overline{\gamma}\pi} e^{\frac{\overline{\gamma}x^2}{4}} Q\left(\sqrt{\frac{\overline{\gamma}x^2}{2}}\right). \tag{61}$$

Finally to summarize all these cases and special cases, we note that from the generic expression of $\mathcal{I}$ and $\mathcal{I}'$ in (51) and (52), one can get the ASER of MPSK over any type of fading covered by the EGK distribution, corrupted by AWLN, and get a simplified expression by doing the necessary manipulations.

As a conclusion, Table I summarize all these cases and define the generic integral $\mathcal{I}$ and its derivative.

F. High SNR Asymptotic Results

It seems interesting to explore an asymptotic study of the SER for high SNR. Because the SER is expressible in terms of the FHF, the known results of the asymptotic expansion of the FHF, near zero (i.e. for high SNR $\overline{\gamma}$), could be used to write down the asymptotic expression of the SER for high SNR in presence of EGK fading. As the SER is totally defined by knowing $\mathcal{I}(x)$, an asymptotic expression of $\mathcal{I}(x)$ is studied for the different fading channels seen above. In fact, from (51) and [29, Eq. (1.8.4)], we have

$$\mathcal{I}(x) = \begin{cases} \frac{2\xi\Gamma\left(m_s - m\frac{\xi}{\xi_s}\right)\Gamma(2m\xi)}{\Gamma(m)\Gamma(m_s)} \left(\frac{\beta_s\beta}{\overline{\gamma}x^2}\right)^{m\xi} & \text{if } \mathrm{m_s}\xi_\mathrm{s} - \mathrm{m}\xi \geq 0 \\ \frac{2\xi_s\Gamma\left(m - m_s\frac{\xi_s}{\xi}\right)\Gamma(2m_s\xi_s)}{\Gamma(m)\Gamma(m_s)} \left(\frac{\beta_s\beta}{\overline{\gamma}x^2}\right)^{m_s\xi_s} & \text{otherwise.} \end{cases} \tag{62}$$

This asymptotic expression is more simplified than the general expression (51). Its derivative can also be easily found as its dependence on x is very simple. Finally, such expression of $\mathcal{I}(x)$ in the selected special cases of fading are summarized in Table II.

V. Numerical and Simulation Results

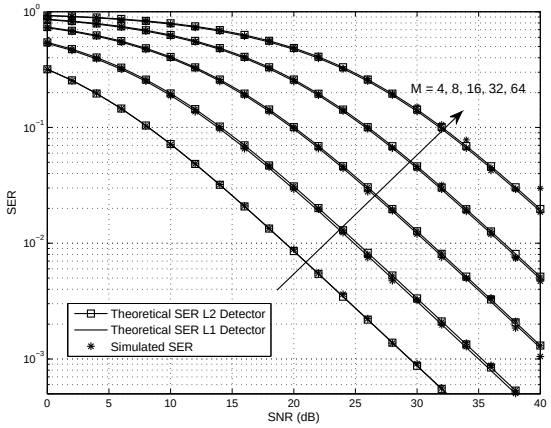

Fig. 7: Difference between the L_1 norm and the L_2 norm detectors in a Rayleigh fading environment (stars denote the simulation results for both detectors).

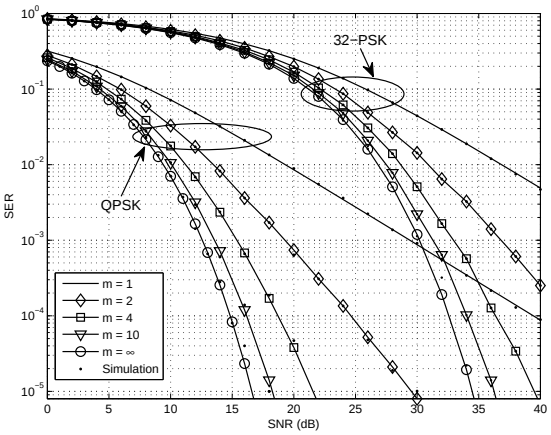

Fig. 8: Comparison between different type of Nakagami fading severity for two constellations (QPSK and 32-PSK). The lines represent the analytical results while the dots denote the simulation results.

This article has been accepted for publication in a future issue of this journal, but has not been fully edited. Content may change prior to final publication. Citation information: DOI 10.1109/TCOMM.2015.2438813, IEEE Transactions on Communications

Table I: $\mathcal{I}(x)$ and $\mathcal{I}'(x)$ for Different Channels

Fading Distribution	$\mathcal{I}(x)$	$\mathcal{I}'(x)$
No Fading	$e^{-x\sqrt{\overline{\gamma}}}$	$-\sqrt{\overline{\gamma}}e^{-x\sqrt{\overline{\gamma}}}$
Rayleigh	$1-\sqrt{\frac{\overline{\gamma}x^2\pi}{}}e^{\frac{\overline{\gamma}x^2}{4}}Q\left(\sqrt{\frac{\overline{\gamma}x^2}{2}}\right)$	$\frac{1}{2}\overline{\gamma}x-\frac{1}{2}(2+\overline{\gamma}x^2)\sqrt{\overline{\gamma}\pi}e^{\frac{\overline{\gamma}x^2}{4}}Q\left(\sqrt{\frac{\overline{\gamma}x^2}{2}}\right)$
Nakagami-m	$\frac{2\Gamma(2m)}{4^m\Gamma(m)}U\left(m,\frac{1}{2},\frac{\overline{\gamma}x^2}{4m}\right)$	$-\frac{\Gamma(2m)\overline{\gamma}x}{4^m\Gamma(m)}U\left(m+1,\frac{3}{2},\frac{\overline{\gamma}x^2}{4m}\right)$
Generalized Nakagami-m	$\frac{2}{\Gamma(m)}\mathrm{H}_{1,1}^{1,1}\left[\frac{\beta}{\overline{\gamma}x^2}\middle\vert\begin{matrix}(1,2)\\(m,\frac{1}{\xi})\end{matrix}\right]$ $=\frac{2\xi}{\Gamma(m)}\left(\frac{\beta}{x^2\overline{\gamma}}\right)^{m\xi}\Gamma\left(2m\xi,0;\left(\frac{\beta}{x^2\overline{\gamma}}\right)^{\xi};-2\xi\right)$	$\frac{-2}{x\Gamma(m)}\mathrm{H}_{1,1}^{1,1}\left[\frac{\beta}{\overline{\gamma}x^2}\middle\vert\begin{matrix}(0,2)\\(m,\frac{1}{\xi})\end{matrix}\right]$ $=\frac{-2\xi}{x\Gamma(m)}\left(\frac{\beta}{x^2\overline{\gamma}}\right)^{m\xi}\Gamma\left(1+2m\xi,0;\left(\frac{\beta}{x^2\overline{\gamma}}\right)^{\xi};-2\xi\right)$
Generalized-K	$\frac{1}{\Gamma(m_s)\Gamma(m)\sqrt{\pi}}\mathrm{G}_{2,2}^{2,2}\left[\frac{4mm_s}{\overline{\gamma}x^2}\middle\vert\begin{matrix}1,1/2\\m,m_s\end{matrix}\right]$	$\frac{-2}{x\Gamma(m_s)\Gamma(m)\sqrt{\pi}}\mathrm{G}_{2,2}^{2,2}\left[\frac{4mm_s}{\overline{\gamma}x^2}\middle\vert\begin{matrix}0,1/2\\m,m_s\end{matrix}\right]$
EGK	$\frac{2}{\Gamma(m_s)\Gamma(m)}\mathrm{H}_{1,2}^{2,1}\left[\frac{\beta_s\beta}{\overline{\gamma}x^2}\middle\vert\begin{matrix}(1,2)\\(m_s,\frac{1}{\xi_s}),(m,\frac{1}{\xi})\end{matrix}\right]$	$\frac{-2}{x\Gamma(m_s)\Gamma(m)}\mathrm{H}_{1,2}^{2,1}\left[\frac{\beta_s\beta}{\overline{\gamma}x^2}\middle\vert\begin{matrix}(0,2)\\(m_s,\frac{1}{\xi_s}),(m,\frac{1}{\xi})\end{matrix}\right]$

Table II: Asymptotic Expansion of $\mathcal{I}(x)$ and $\mathcal{I}'(x)$ for Different Channels

Fading Type	$\mathcal{I}(x)$	$\mathcal{I}'(x)$	Condition
Rayleigh	$\frac{2}{\overline{\gamma}x^2}$	$-\frac{4}{\overline{\gamma}x^3}$	
Nakagami-m	$\frac{2\Gamma(2m)}{\Gamma(m)}\left(\frac{m}{\overline{\gamma}x^2}\right)^m$	$-\frac{4m\Gamma(2m)}{x\Gamma(m)}\left(\frac{m}{\overline{\gamma}x^2}\right)^m$	
GNM	$\frac{2\xi\Gamma(2m\xi)}{\Gamma(m)}\left(\frac{\beta}{\overline{\gamma}x^2}\right)^{m\xi}$	$-\frac{4m\xi^2\Gamma(2m\xi)}{x\Gamma(m)}\left(\frac{\beta}{\overline{\gamma}x^2}\right)^{m\xi}$	
Generalized-K	$\frac{2\Gamma(m-m_s)\Gamma(2m_s)}{\Gamma(m)\Gamma(m_s)}\left(\frac{m_sm}{\overline{\gamma}x^2}\right)^{m_s}$	$-\frac{4m_s\Gamma(m-m_s)\Gamma(2m_s)}{x\Gamma(m)\Gamma(m_s)}\left(\frac{m_sm}{\overline{\gamma}x^2}\right)^{m_s}$	$m\geq m_s$
	$\frac{2\Gamma(m_s-m)\Gamma(2m)}{\Gamma(m)\Gamma(m_s)}\left(\frac{m_sm}{\overline{\gamma}x^2}\right)^{m}$	$-\frac{4m\Gamma(m_s-m)\Gamma(2m)}{x\Gamma(m)\Gamma(m_s)}\left(\frac{m_sm}{\overline{\gamma}x^2}\right)^{m}$	$m_s\geq m$
EGK	$\frac{2\xi_s\Gamma\left(m-m_s\frac{\xi_s}{\xi}\right)\Gamma(2m_s\xi_s)}{\Gamma(m)\Gamma(m_s)}\left(\frac{\beta_s\beta}{\overline{\gamma}x^2}\right)^{m_s\xi_s}$	$-\frac{4m_s\xi_s^2\Gamma\left(m-m_s\frac{\xi_s}{\xi}\right)\Gamma(2m_s\xi_s)}{x\Gamma(m)\Gamma(m_s)}\left(\frac{\beta_s\beta}{\overline{\gamma}x^2}\right)^{m_s\xi_s}$	$m\xi\geq m_s\xi_s$
	$\frac{2\xi\Gamma\left(m_s-m\frac{\xi}{\xi_s}\right)\Gamma(2m\xi)}{\Gamma(m)\Gamma(m_s)}\left(\frac{\beta_s\beta}{\overline{\gamma}x^2}\right)^{m\xi}$	$-\frac{4m\xi^2\Gamma\left(m_s-m\frac{\xi}{\xi_s}\right)\Gamma(2m\xi)}{x\Gamma(m)\Gamma(m_s)}\left(\frac{\beta_s\beta}{\overline{\gamma}x^2}\right)^{m\xi}$	$m_s\xi_s\geq m\xi$

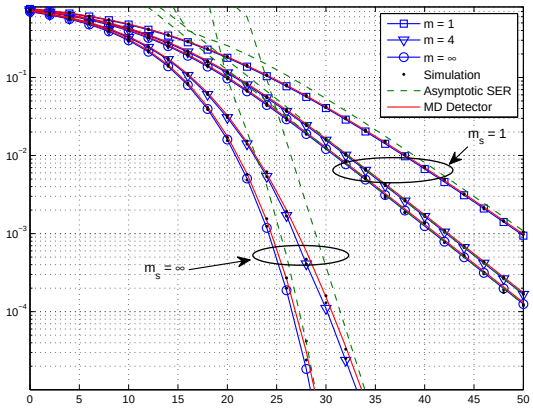

Fig. 9: Comparison between ML and MD detectors in Generalized-K fading for 16-PSK. The lines represent the analytical results, while the dots denote the simulation results, and the dashed lines represent the asymptotic results for high SNR.

In this section, we perform some numerical results to investigate the system performance by drawing the SER and the ASER versus the received SNR and for different size of the MPSK constellation. Moreover, some types of fading are tested to see the impact of the channel on the system performance.

In Fig. 7, we compare the system performance of both the ML and MD detectors. This illustration is an extension of the results presented in Fig. 5 since the ASER of the system over Rayleigh fading is drawn with the conditional SER. In both cases we draw the SER for 4, 8, 16, 32, and 64 PSK. From a mathematical point of view, and from the simulation results, both detectors give the same results in QPSK case. However for $M \geq 8$ there is a small difference between the two detectors with a little advantage to the ML detector (as described in subsection III-C). Furthermore, it is clear that by increasing M the gap is going down. In the ideal case (without fading), the gap is clear and it is less than 1dB for all cases. However in Rayleigh fading case, the curves are very close and the gap becomes very small (< 0.3dB), and by increasing M the curves get close to each other. For example for 64-PSK the ML and MD detectors have approximately the same performance.

On the other hand it is clear that the system performance improves by decreasing the constellation size M. Also the SER is better in the environment without fading than in the Rayleigh fading case. One more remark is that the numerical results match perfectly the simulation results.

Fig. 8 shows the system performance in the presence of a Nakagami-m fading for different values of m, considering the QPSK and 32-PSK constellations, and using ML detector. The first remark that one can conclude is that the simulation results match perfectly with the analytical results. As in the previous figure, the performance in the QPSK case is better than the performance in the 32-PSK case, which is explained

This article has been accepted for publication in a future issue of this journal, but has not been fully edited. Content may change prior to final publication. Citation information: DOI 10.1109/TCOMM.2015.2438813, IEEE Transactions on Communications

by the fact that the distance between the symbols in the QPSK case is bigger than the distance in the 32-PSK case. Looking at the effect of the fading, one can conclude that the SER has better values by increasing m, the fading figure, and the best curves appears for $m \to \infty$ in both cases. In fact for small values of the fading figure (i.e. $m = 1$) the fading dominates the detection error and consequently the probability of error becomes higher. Also by increasing m, the fading effect on the signal decreases and the system becomes without fading for large values of m ($m \to \infty$), which is the best scenario.

In the last illustration, Fig. 9 draws the SER issued from both detectors MD and ML for a generalized-K distribution (i.e. $\xi = 1$ and $\xi_s = 1$) for different values of the figures m and m_s. In fact such results allow us to compare both detectors in the presence of variety of fading severity. Also the asymptotic results for high SNR are drawn, but only using the ML detector, to confirm its utility. It is important to note that the results for $m_s = 1$ and $m = \infty$ (i.e. Rayleigh fading) are the same as $m_s = \infty$ and $m = 1$, so only one case is drawn. Also the case $m_s = \infty$ and $m = \infty$ represents the case without fading. Thereby, it is clear from the figure, that the system performance gets better by increasing the fading and shadowing figures (i.e. reduce the severity of the fading and shadowing). Moreover, it is seen that both detector keep a closer performance even for different values m and m_s. However, we note that for high severity (i.e. $m = 1$ and $m_s = 1$) the difference is negligible relative to the gap in less severity cases ($m_s = \infty$). On the other hand, the asymptotic results for high SNR (dashed lines) show a good approximation for the SER in the treated cases. Finally the simulated results match perfectly the theoretical results which validate again our mathematical model and analytical calculations.

VI. Conclusion

In this paper, the decision regions of an MPSK constellation transmitted over an additive Laplacian noise channel was presented using two detectors, namely the ML and the MD detectors. In addition, closed-form expressions of the ASER in presence of EGK fading were derived in terms of the FHF. These complicated results were simplified for a selected group of special cases and analyzed asymptotically for the high SNR regime. Finally a numerical comparison between these two detectors, backed-up with Monte-Carlo simulations, showed a close performance between them especially for severe fading conditions.

References

[1] N. Beaulieu and B. Hu, "Soft-limiting receiver structures for time-hopping UWB in multiple-access interference," *IEEE Transactions on Vehicular Technology*, vol. 57, no. 2, pp. 810–818, March 2008.

[2] Y. Dhibi and T. Kaiser, "On the impulsiveness of multiuser interferences in TH-PPM-UWB systems," *IEEE Transactions on Signal Processing*, vol. 54, no. 7, pp. 2853–2857, July 2006.

[3] ——, "Impulsive noise in UWB systems and its suppression," *Mobile Networks and Applications, Kluwer Academic Publishers*, vol. 11, no. 4, pp. 441–449, 2006.

[4] J. Xian and Y. Geng, "Multi-user detection based on particle filter in impulsive noise," *International Journal of Advancements in Computing Technology*, vol. 5, no. 4, p. 259, Feb. 2013.

[5] S. Bernstein, M. Burrows, J. Evans, A. Griffiths, D. McNeill, C. Niessen, I. Richer, D. White, and D. Willim, "Long-range communications at extremely low frequencies," *Proceedings of the IEEE*, vol. 62, no. 3, pp. 292–312, March 1974.

[6] B. Hu and N. Beaulieu, "On characterizing multiple access interference in TH-UWB systems with impulsive noise models," in *Proc. of the IEE Radio and Wireless Symposium*, Orlando, FL, USA, Jan. 2008, pp. 879–882.

[7] ——, "Accurate evaluation of multiple-access performance in TH-PPM and TH-BPSK UWB systems," *IEEE Transactions on Communications*, vol. 52, no. 10, pp. 1758–1766, Oct. 2004.

[8] J. Fiorina, "A simple IR-UWB receiver adapted to multi-user interferences," in *Proc. of the IEEE Global Telecommunications Conference (GLOBECOM'2006)*, San Francisco, CA, USA, Nov. 2006, pp. 1–4.

[9] S. Jiang and N. Beaulieu, "BER of antipodal signaling in Laplace noise," in *Proc. of the 25th Biennial Symposium on Communications (QBSC'2010)*, Kingston, ON, Canada, May 2010, pp. 110–113.

[10] G. Durisi and G. Romano, "On the validity of Gaussian approximation to characterize the multiuser capacity of UWB TH PPM," in *Proc. of the IEEE Conference on Ultra Wideband Systems and Technologies*, Baltimore, MD, USA, May 2002, pp. 157–161.

[11] N. C. Beaulieu and D. J. Young, "Designing time-hopping ultrawide bandwidth receivers for multiuser interference environments," *Proceedings of the IEEE*, vol. 97, no. 2, pp. 255–284, Feb. 2009.

[12] M. Chiani and A. Giorgetti, "Coexistence between UWB and narrowband wireless communication systems," *Proceedings of the IEEE*, vol. 97, no. 2, pp. 231–254, Feb. 2009.

[13] Q. Ahmed, K.-H. Park, and M.-S. Alouini, "Ultrawide Bandwidth receiver based on a multivariate generalized Gaussian distribution," *IEEE Transactions on Wireless Communications*, vol. PP, no. 99, pp. 1–1, 2014.

[14] A. Kamboj, R. Mallik, M. Agrawal, and R. Schober, "Diversity combining in FSO systems in presence of non-Gaussian noise," in *Proc. of the International Conference on Signal Processing and Communications (SPCOM), Bangalore, India*, July 2012, pp. 1–5.

[15] N. C. Beaulieu, G. Bartoli, D. Marabissi, and R. Fantacci, "The structure and performance of an optimal continuous-time detector for Laplace noise," *IEEE Communications Letters*, vol. 17, no. 6, pp. 1065–1068, June 2013.

[16] H. Shao and N. C. Beaulieu, "An investigation of block coding for Laplacian noise," *IEEE Transactions on Wireless Communications*, vol. 11, no. 7, pp. 2362–2372, July 2012.

[17] S. Jiang and N. C. Beaulieu, "Precise BER computation for binary data detection in bandlimited white Laplace noise," *IEEE Trans. Commun.*, vol. 59, no. 6, pp. 1570–1579, Jun. 2011.

[18] C. W. Helstrom, "Detectability of signals in Laplace noise," *IEEE Trans. Aerosp. Electron. Syst.*, vol. 25, no. 2, pp. 190–196, Mar. 1989.

[19] M. W. Thompson and H.-S. Chang, "Coherent detection in Laplace noise," *IEEE Trans. Aerosp. Electron. Syst.*, vol. 30, no. 2, pp. 452–461, Apr. 1994.

[20] D. Yoon, "New expression for the SER of M-ary PSK," *IEICE Transactions*, vol. 88-B, no. 4, pp. 1672–1676, Apr. 2005.

[21] H. Soury and M.-S. Alouini, "On the symbol error rate of M-ary MPSK over generalized fading channels with additive Laplacian noise," in *Proc. of the IEEE International Symposium on Information Theory (ISIT'2014)*, Honolulu, Hawai, USA, June 2014, pp. 2879–2883.

[22] R. K. Mallik, A. K. Gogoi, A. Mahanta, and R. Raghuram, "Analysis of performance of BPSK in an additive combination of impulsive and Gaussian noise," *Wireless Personal Communications*, vol. 26, no. 1, pp. 1–15, Aug. 2003.

[23] F. Yilmaz and M.-S. Alouini, "A new simple model for composite fading channels: Second order statistics and channel capacity," in *Proc. of the IEEE 7th International Symposium on Wireless Communication Systems (ISWCS'2010), York, UK*, Sept. 2010, pp. 676–680.

[24] H. Soury, F. Yilmaz, and M.-S. Alouini, "Error rates of M-PAM and M-QAM in generalized fading and generalized Gaussian noise environments," *IEEE Communications Letters*, vol. 17, no. 10, pp. 1932–1935, October 2013, Extended version available as technical report at http://hdl.handle.net/10754/294163.

[25] I. Marks, R.J., G. Wise, D. Haldeman, and J. Whited, "Detection in Laplace noise," *IEEE Transactions on Aerospace and Electronic Systems*, vol. AES-14, no. 6, pp. 866–872, Nov. 1978.

[26] S. Kotz, T. Kozubowski, and K. Podgórski, *The Laplace Distribution and Generalizations: A Revisit With Applications to Communications, Exonomics, Engineering, and Finance*, ser. Progress in Mathematics Series. Springer Verlag, N.Y., 2001.

[27] H. Soury, F. Yilmaz, and M.-S. Alouini, "Average bit error probability of binary coherent signaling over generalized fading channels subject to additive generalized Gaussian noise," *IEEE Commun. Lett.*, vol. 16, no. 6, pp. 785–788, June 2012.

[28] M. A. Chaudhry and S. M. Zubair, *On a Class of Incomplete Gamma Function with Applications*. Boca Raton-London-Ney York-Washington, D.C.: Chapman & Hall/CRC, 2002.

[29] A. Kilbas and M. Saigo, *H-Transforms : Theory and Applications (Analytical Method and Special Function)*, 1st ed. CRC Press, 2004.

[30] A. P. Prudnikov, Y. A. Brychkov, and O. I. Marichev, *Integral and Series: Volume 3, More Special Functions*. CRC Press Inc., 1990.

[31] F. Yilmaz and M.-S. Alouini, "Product of the powers of generalized Nakagami-m variates and performance of cascaded fading channels," in *Proc. of the IEEE Global Telecommunication Conference (GLOBECOM'2009), Honolulu, Hawai, USA*, Dec 2009, pp. 1–8.

[32] ——, "A unified MGF-based capacity analysis of diversity combiners over generalized fading channels," *IEEE Transactions on Communications*, vol. 60, no. 3, pp. 862–875, March 2012.

[33] M. Abramowitz and I. A. Stegun, *Handbook of Mathematical Functions with Formulas, Graphs, and Mathematical Tables*, ser. National Bureau of Standards Applied Mathematics Series. New York: Dover Publications, 1964.